

A comparative study of forming limit diagram prediction of tailor welded blanks

R. Safdarian · R. M. Natal Jorge · Abel D. Santos ·
H. Moslemi Naeini · M. P. L. Parente

Received: 9 October 2013 / Accepted: 18 March 2014 / Published online: 8 April 2014
© Springer-Verlag France 2014

Abstract The Forming Limit Diagram (FLD) is a useful method for characterizing the formability of sheet metals. In this paper, different numerical models were used to investigate the FLD of Tailor Welded Blanks (TWB). TWB were CO₂ laser-welded of interstitial-free (IF) steel sheets with difference in thickness. Numerical approaches of Müschenborn-Sonne Forming Limit Diagram (MSFLD), Forming Limit Diagram criterion (FLD_{crt}) and Ductile Fracture Criterion (DFC_{crt}), as well as new numerical method of Second Derivative of Thinning (SDT) were used for FLD prediction. The results of numerical models were compared with the experimental FLD, Limit Dome Height (LDH) and also load–displacement of samples. The emphasis of this investigation is to determine the performance of these different approaches in predicting the FLD. Results show that previous approaches are successful for the left side of FLD (drawing), but not so successful for the right side of the FLD (stretching). Influence of anisotropy on the forming behavior of TWB is investigated in this study and its results are compared with isotropic models and experimental data.

Keywords Tailor welded blank (TWB) · Ductile fracture criteria · Forming limit diagram · Finite element method (FEM)

R. Safdarian (✉)
Department of Mechanical Engineering, Behbahan Khatam Alanbia
University of Technology, P.O. Box: 6361647189 Behbahan,
Khoozestan, Iran
e-mail: safdarian@bkatu.ac.ir

R. M. N. Jorge · M. P. L. Parente
IDMEC, Faculty of Engineering, University of Porto, Porto, Portugal

A. D. Santos
INEGI, Faculty of Engineering, University of Porto, Porto, Portugal

H. M. Naeini
Department of Mechanical engineering, Tarbiat Modares University,
Tehran, Iran

Introduction

Prediction of the forming limits in sheet metal forming is very important in order to identify the conditions that may lead to necking and fracture. The forming limit curve at necking (FLCN) is used as a criterion for prediction of sheet metal forming limit. It displays in principal strain space (major and minor strains) at the onset of local necking. On the other hand, the forming limit curve at fracture (FLCF) is defined by the combined principal strains up to fracture. Figure 1 indicates the schematic diagrams showing the FLCN and FLCF. Here, $\alpha (=d\sigma_2/d\sigma_1)$ defines stress ratio and $\rho (=d\epsilon_2/d\epsilon_1)$ is the strain ratio. For a given initial strain path, after the onset of strain localization, the material deforms in restricted area and follows an almost plane strain path up to failure [1].

FLD of sheet metals was initially characterized by Keeler and Backofen [2] and Goodwin [3] and later became industrial practice as well as a topic of research, both theoretically and experimentally. Since then, a lot of research has been performed for calculation of FLCN and FLCF. Forming limit diagrams at necking and at fracture for AA6111-T4 sheet material were experimentally determined by Jain et al. [4], and surfaces of fractured dome specimens were observed by optical microscopy and by Scanning Electron Microscope (SEM). Ozturk and Lee [5] obtained the limit strains for FLD by substituting stress and strain values obtained from the finite element (FE) simulation of out-of-plane formability test into the ductile fracture criterion.

A Tailor-Welded Blank (TWB) consists of steels with different thicknesses or strength types welded together to produce a single blank, prior to the forming process. Automotive designers are always looking for new technologies to reduce vehicle weight and manufacturing costs in order to meet ever restricting fuel economy standards while remaining economically competitive. An opportunity to meet these seemingly conflicting requirements is through the use of Tailor-Welded Blanks (TWBs) [6].

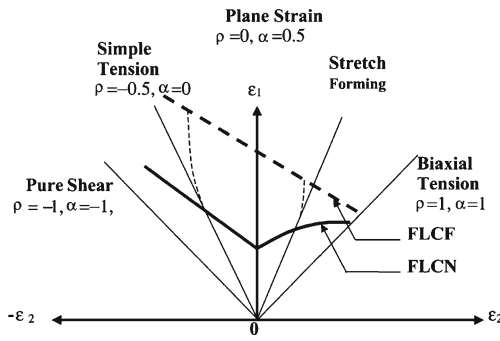


Fig. 1 Schematic diagram showing the FLCN and FLCF

Many recent studies on the tailored blanks are focused mainly on the formability and applications of TWB. Shi et al. [7] studied the optimal conditions for laser and mash-seam welding to obtain better formability of tailored blanks. Chien et al. [8] employed a bifurcation criterion to estimate the onset of failure in transversely loaded AA5754 TWBs. In their analysis, a FE model, representing the geometrical configuration, was combined with an analytical model to predict failure. Chan et al. [9] found that higher the thickness ratio, the lower was the level of FLD. The findings also showed that minimum major strain of FLD (FLD_0) decreases with increase in thickness ratio. Safdarian Korouyeh et al. [10] investigated performance of different numerical criteria for FLD prediction of TWB. Second Derivative of Thinning (SDT) was found as a good post-processing criterion for FLD prediction of TWB. They also study the effect of thickness ratio on the level of FLD for St12 TWB with different thickness ratio in another research [11]. Their results showed that FLD’s level increase by thickness ratio decreasing of TWB.

In the present work different numerical approaches were used to predict the FLD of IF steel TWB. These methods contained: Müschenborn and Sonne Forming Limit Diagram (MSFLD), Forming Limit Diagram criterion (FLDcrt), Second Derivative of Thinning (SDT) and Ductile Fracture Criterion (DFCrt).

Hill’s anisotropic yield criterion and Holloman hardening model were used to model the behavior of metals. Influence of anisotropy on the forming behavior of TWB was also investigated in this research. FLDs of numerical models were compared with the experimental results, as well as LDH and load–displacement curves of numerical criteria. Results show a good agreement between numerical analysis and experiments.

FLD criteria

MSFLD, FLDcrt and DFCrt (Abaqus® 6.10) and SDT criteria were used for prediction of TWB’s FLD. SDT is a post processing numerical criterion. M-K (Marciniak-Kuczynski) criterion, which also may be used in Abaqus, is implemented just for isotropic materials. It is not considered in this research, because anisotropy is an important parameter to be included

in this research. The fundamentals of these criteria are presented, in order to understand and relate corresponding behavior and results.

MSFLD criterion

Müschenborn and Sonne [12] proposed a method to predict the influence of the deformation path on the forming limits of sheet metals on the basis of the equivalent plastic strain, by assuming that the forming limit diagram represents the sum of the highest attainable equivalent plastic strains. A generalization of this idea permits establishing a criterion of necking instability of sheet metals for arbitrary deformation paths. The approach requires transforming the original forming limit diagram (without predeformation effects) from the space of major versus minor strains to the space of equivalent plastic strain, $\bar{\epsilon}^{pl}$, versus ratio of principal strain rates, $\rho = \dot{\epsilon}_2/\dot{\epsilon}_1$.

For linear strain paths and anisotropic material, assuming plastic incompressibility and neglecting elastic strains:

$$\rho = \epsilon_2 / \epsilon_1 \tag{1}$$

$$\bar{\epsilon}^{pl} = \frac{1 + R}{\sqrt{1 + 2R}} \sqrt{\epsilon_1^2 + \epsilon_2^2} + \frac{2R}{1 + R} \epsilon_1 \epsilon_2 \tag{2}$$

where ϵ_1 and ϵ_2 are the major and minor strain, respectively and should be calculated by experimental out-of-plane tests. Indeed these are the values of experimental FLD. These values of strains and ρ value were measured from the necking element. R is the normal anisotropy and can be calculated by following equation:

$$R = \frac{r_0 + 2r_{45} + r_{90}}{4} \tag{3}$$

where r_0 , r_{45} and r_{90} are anisotropic parameters in 0, 45 and 90°, respectively. These parameters were calculated experimentally using ASTM-E517 test [13].

For the specification of the MSFLD damage initiation criterion in Abaqus, ρ and equivalent plastic strain at damage initiation were calculated by Eq. (1) and Eq. (2) respectively, based on experimental FLD of this research.

In MSFLD criterion, ω_{MSFLD} represent the ratio of the current equivalent plastic strain, $\bar{\epsilon}^{pl}$, to the equivalent plastic strain on the limit curve. The necking instability is met when the condition $\omega_{MSFLD}=1$ is satisfied. First element in which $\omega_{MSFLD}=1$ is selected as necking element and corresponding major and minor strains defined a point on FLD.

FLDcrt criterion

The maximum strains that a sheet material can sustain prior to the onset of necking are referred as forming limit strains. A

FLD is a plot of the forming limit strains in the space of principal strains. The necking initiation criterion for the FLD_{crt} is given by the condition $\omega_{FLD}=1$, where the variable ω_{FLD} is a function of the current deformation state and is defined as the ratio of the current major principal strain, ϵ_1 , to the major limit strain on the FLD evaluated at the current values of the minor principal strain, ϵ_2 .

In this research experimental FLD of TWB was imported to FE code as FLD_{crt}. Experimental FLD was based on the major and minor strains which were measured from the experimental samples of present study. This FLD was used in the Abaqus software to predict the necking defects in the FEM samples. After completion of simulations, first element which $\omega_{FLD}=1$, was considered as necking element and its major and minor strains were used to define a point on FLD. This test was performed for all samples. Load and displacement of the punch at necking based on FLD_{crt} criterion were compared with other criteria and also with experiment.

Second derivative of thinning (SDT) criterion

Material thinning can be a criterion for necking. Using Brun’s idea, time and spatial necking of a particular specimen can be predicted based on the second derivative of thinning [14]. Considering this model, thickness of all elements of FEM model were analyzed in order to determine minimal thickness for each stored time interval. Thinning values for all elements with minimal thickness were stored and finally, second derivative of thinning was analyzed. Due to a fast local change of sheet thickness at the necking point, the thickness strain changes abruptly its value. The acceleration of thickness deformation (second time derivative) is defined as

$$\ddot{\epsilon}_{33} = \frac{d^2 \epsilon_{33}}{dt^2} \tag{4}$$

where ϵ_{33} is the thickness strain of element. The element at which the peak of $\ddot{\epsilon}_{33}$ first appeared (at minimal time) was assumed as the element which the onset of necking started and the time of this peak was considered as necking time. The major and minor strains for this element at necking time defined a point of FLD and this trend was repeated for all samples. More details about this criterion are available in [10]. Figure 2 shows the second derivative of thinning for necking element of sample with 200 mm width. This figure shows that SDT of this element has a peak in the 0.038 s of simulation time. Based on this criterion, major and minor strain of necking element for this simulation instance is considered as a point of FLD.

Ductile fracture criterion (DFC_{crt})

The fracture of ductile materials is mainly due to growth and coalescence of microscopic voids existing within the material.

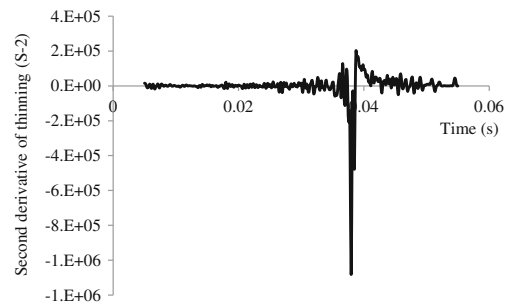


Fig. 2 SDT of necking element for 200 mm×200 mm sample

In the numerical simulation, when the fracture threshold within an element is reached, that element fractures and a crack occurs. This model assumes that the equivalent plastic strain at the onset of damage, $\bar{\epsilon}_D^{pl}$, is a function of stress triaxiality and strain rate

$$\bar{\epsilon}_D^{pl} \left(\eta, \dot{\bar{\epsilon}}^{pl} \right) \tag{5}$$

where η is stress triaxiality and $\dot{\bar{\epsilon}}^{pl}$ is the equivalent plastic strain rate.

The criterion for damage initiation is met when the following condition is satisfied:

$$\omega_D = \int \frac{d\bar{\epsilon}^{pl}}{\bar{\epsilon}_D^{pl} \left(\eta, \dot{\bar{\epsilon}}^{pl} \right)} = 1 \tag{6}$$

and stress triaxiality can be calculated as follow:

$$\eta = \frac{\sigma_m}{\bar{\sigma}_{VM}} = \frac{1/3(\sigma_1 + \sigma_2 + \sigma_3)}{\sqrt{1/2[(\sigma_1 - \sigma_2)^2 + (\sigma_2 - \sigma_3)^2 + (\sigma_3 - \sigma_1)^2]}} \tag{7}$$

where σ_m is mean stress, $\bar{\sigma}_{VM}$ is Mises equivalent stress, $\sigma_1, \sigma_2, \sigma_3$ are principal stresses.

By plane stress assumption $\sigma_3=0$, σ_1 and σ_2 can be calculated from experimental major strain (ϵ_1) and minor strain (ϵ_2). The ratio of the minor true stress, σ_2 , to the major true stress,

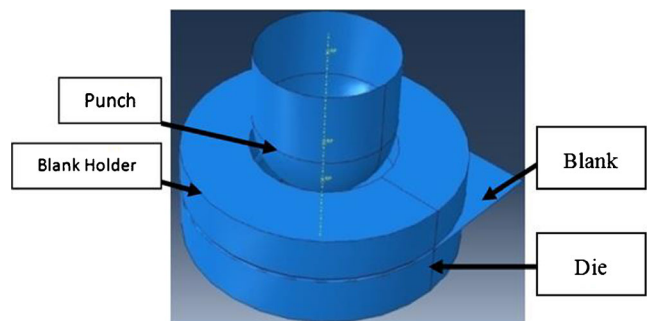
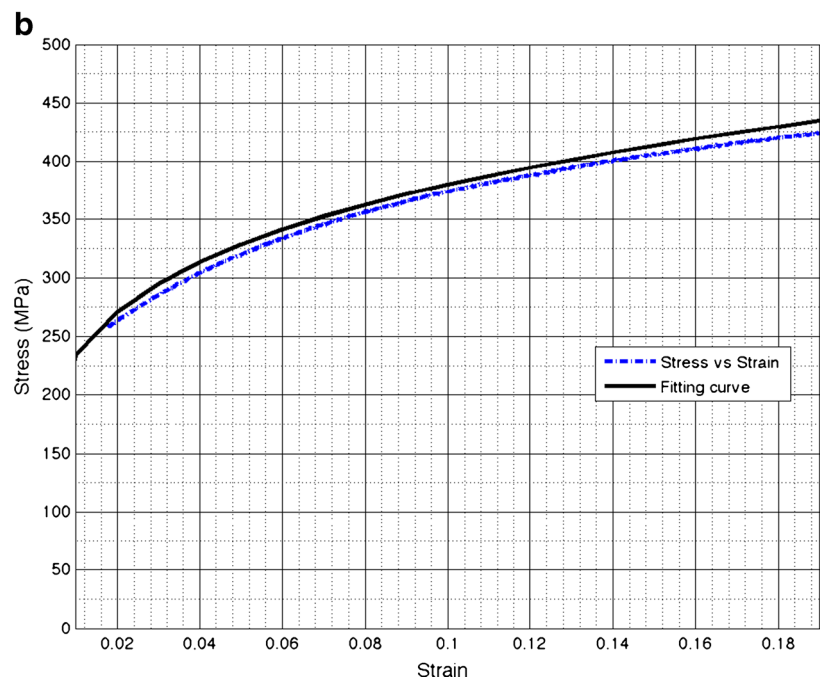
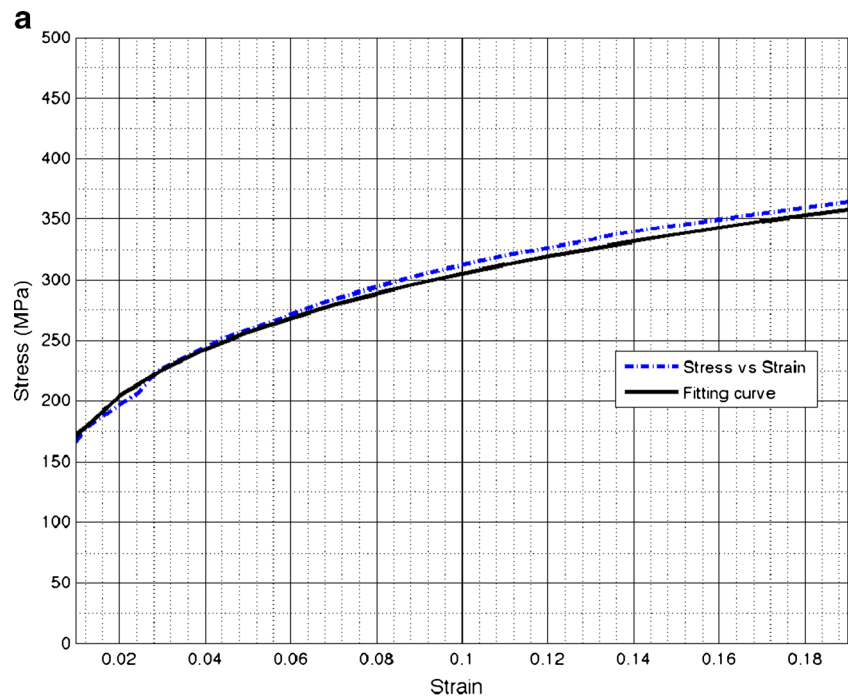


Fig. 3 Setup of tools used in numerical simulation

Table 1 Mechanical properties of IF steel base metals from tensile tests

Sheet thickness (mm)	YS(N/mm ²)	UTS (N/mm ²)	Elongation (%)	n	K(N/mm ²)	R ²	Anisotropy parameter		
							r ₀	r ₄₅	r ₉₀
0.77	156	302	47	0.25	542.4	0.9653	1.94	1.8	2.73
1.17	225	340	40	0.21	616	0.9967	1.81	1.64	2.54

Fig 4 Curve fitting of strain–stress curve for IF steel with thickness of **a** 0.77 mm and **b** 1.17 mm

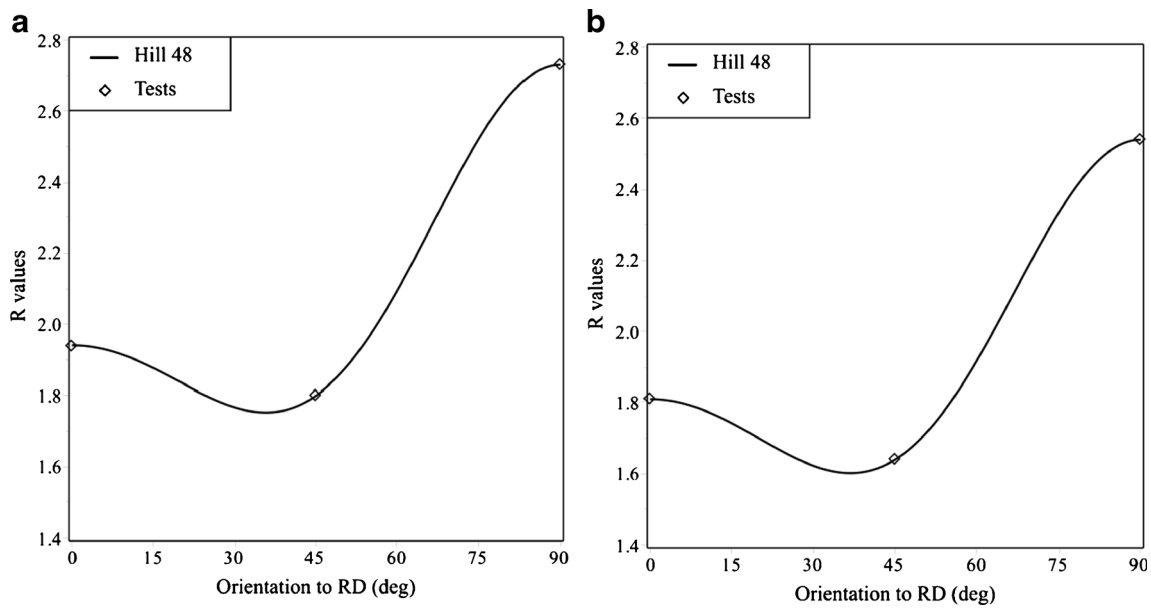


Fig 5 Variation of R-value vs. rolling direction for **a** 0.77 mm and **b** 1.17 mm

σ_1 , is defined by the parameter

$$\alpha = \frac{\sigma_2}{\sigma_1} \tag{8}$$

By Eq. (1), Eq. (8), normal anisotropy assumption for sheet and flow rule, the relation between α and ρ is as follow:

$$\alpha = \frac{(1 + R)\rho + R}{1 + R + R\rho} \tag{9}$$

Plasticity theory defines an effective stress, $\bar{\sigma}$, which is a function of the stress tensor components and a set of material parameters. For materials with normal anisotropy and zero shear stress in a coordinate system aligned with the anisotropy, the definition of the effective stress can be expressed in terms of the principal stresses

$$\bar{\sigma} = \sqrt{\sigma_1^2 + \sigma_2^2 - \frac{2R}{1+R}\sigma_1\sigma_2} \tag{10}$$

This relation can also be expressed in terms of σ_1 and α

$$\bar{\sigma} = \sigma_1 \xi(\alpha) \Rightarrow \sigma_1 = \frac{\bar{\sigma}}{\xi(\alpha)} \tag{11}$$

where $\xi(\alpha)$ is a function of material parameters and can be calculated as follow

$$\xi = \sqrt{1 + \alpha^2 - \frac{2R}{1+R}\alpha} \tag{12}$$

α is calculated by Eq. (9) and using major and minor strains from experimental FLD; the relation between the effective stress and effective strain can be written

formally as

$$\bar{\sigma} = \bar{\sigma}(\bar{\epsilon}) \tag{13}$$

The most commonly used representation of this relation is the power law

$$\bar{\sigma} = K\bar{\epsilon}^n \tag{14}$$

where K and n are material constants and $\bar{\epsilon}$ can be calculated from Eq. (2). By substituting Eqs. 14 and 12 into Eq. (11), σ_1 is obtained. Then σ_2 is calculated by Eq. (8) and using σ_1 , σ_2 and plane stress condition, η is obtained by Eq. (7). When importing DFCrt to FE code two parameters of stress triaxiality and fracture strain are needed, in which fracture strain is equivalent to fracture strain at damage initiation. Equivalent fracture strain at damage initiation, $\bar{\epsilon}^{pl}$, can be calculated by Eq. (2). First element which $\omega_D=1$ is selected as necking element and major and minor strains of such element is imported to the forming limit diagram.

Numerical investigation

Numerical investigation of stretch forming of tailor welded blanks was done using a commercially available finite element

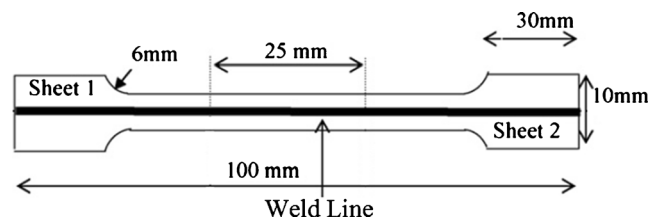


Fig 6 Sub-size TWB tensile specimen used in ASTM-E8 test

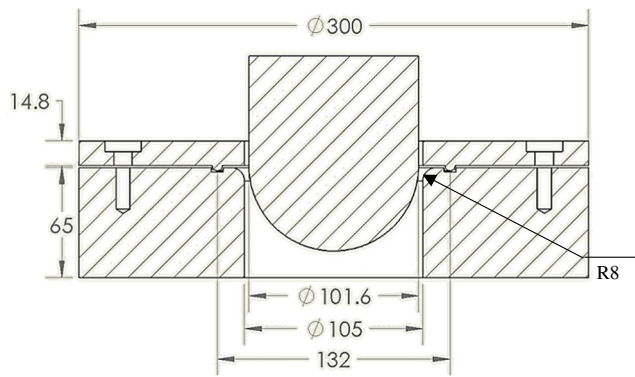


Fig 7 A schematic of the tools used in stretch forming experiments (all dimensions in mm)

code Abaqus/Explicit 6.10. The FEM model consisted of a hemispherical punch, blank holder, die and the blank as shown in Fig. 3. Punch, die and blank holder were modeled as analytical rigid parts, because one considers they have negligible deformation. The blank was modeled as a deformable part using four node Kirchhoff thin shell elements (S4R). The circular draw-bead model is obtained by constraint forces applied on a circular partition of sheet at a distance of 66 mm from the center of the die. The coefficient of friction at the tool-blank contact was considered as 0.15, based on the works of Panda et al. [15]. The die was fixed and the punch was moved downward with a numerical speed of 1,000 mm/s. This speed was selected based on the quasi static condition of forming process [16]. This velocity was also used by Panda et al. [15] for punch movement in the stretch forming.

TWB consisted of a blank with two IF steel with thicknesses of 0.77 mm and 1.17 mm. Mechanical properties of base metals are shown in Table 1. These mechanical properties are Yield Stress (YS), Ultimate Tensile Strength (UTS), work hardening exponent (n), work hardening coefficient and elongation. Hollomon's equation ($\sigma = K\varepsilon^n$) was used to model the plastic behavior of sheet material. The R^2 values of this table show curvature fitting of stress–strain curves related to sheet thickness. For the two thicknesses of the IF sheets, it is found that $R^2 > 0.95$, which indicates the good correlation between

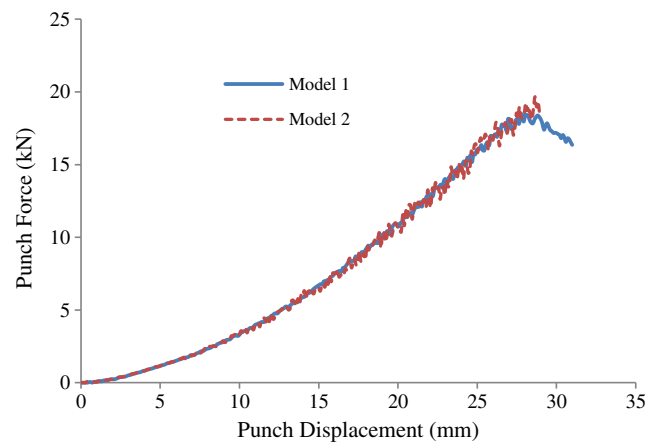


Fig. 9 Load- displacement comparison for models with rough and fine mesh

the curves. Figure 4 shows the fitting of experimental strain–stress curves for the calculation of Hollomon's equation parameters (K and n).

Figure 5 shows the variation of R-value vs. rolling direction for two thicknesses of 0.77 mm and 1.17 mm of IF steel. This figure shows that minimum R-value is in the direction of 45° with the rolling direction.

Laser welding produces a very narrow weld line with small heat affected zone. For better understanding of the effect of weld line on the forming of TWB samples, substandard longitudinal welded tensile specimens were prepared for tensile test from laser welded samples, according to ASTM E8M standard [13], as shown in Fig. 6. A 4 mm width was used for the gauge section, which contains the weld and heat affected zone. This test was done to obtain mechanical properties of the weld. This method was used by Panda et al. [15] for measure the mechanical properties of the weld region.

Mechanical properties of TWB were compared with Table 1 information and shown that there is no high difference between mechanical properties of weld region and base metal. Similar observation and conclusions has been reported by Saunders and Wagoner [17]. For this reason, in the numerical modeling it will be assumed no difference in material

Fig 8 Experimental setup

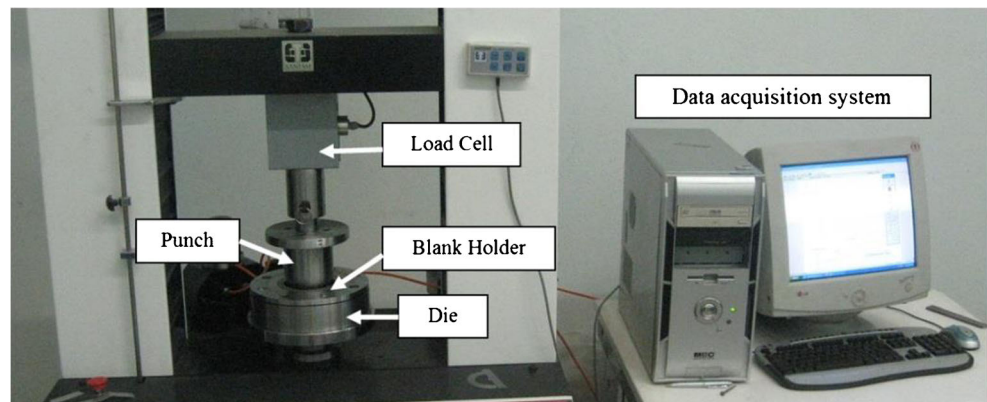


Table 2 Comparison of necking time and limit strains of two models

Mesh size	Necking time (s)	Major strain of necking element	Minor strain of necking element
Model 1 (1mm×1mm)	0.0276	0.295	-0.006
Model 2 (0.5mm×0.5 mm)	0.0273	0.305	-0.009

behavior due to welding, although this should be a subject for further investigation.

The standard eight different strain paths (25×200 to 200×200 mm) were simulated to predict the FLD of welded blank. Different FLD criteria, already presented in Section “FLD criteria”, were used in all simulations. Optimal blank holder force was chosen such that the blank neither draws-in nor tears near draw bead. More details about the numerical analysis are available in [10].

The fracture behavior of cold rolled sheet metals is influenced by the anisotropy of mechanical properties due to

crystallographic texture. In this research blank was modeled both as isotropic as well as anisotropic to show the influence of anisotropy on the forming results. Load-displacements curves of these models were compared with each other and with experiment. Many phenomenological yield criteria have been proposed in the past to account for plastic anisotropy, among which Hill’s quadratic yield criterion [18] has been widely used, while being well adapted for steel sheets. Therefore in this research Hill’s 1948 yield criterion is used to model sheet metal behavior in forming process.

$$f(\sigma) = \sqrt{F(\sigma_{22}-\sigma_{33})^2 + G(\sigma_{33}-\sigma_{11})^2 + H(\sigma_{11}-\sigma_{22})^2 + 2L\sigma_{23}^2 + 2M\sigma_{31}^2 + 2N\sigma_{12}^2} \tag{15}$$

$$\begin{aligned} F &= \frac{1}{2} \left(\frac{1}{R_{22}^2} + \frac{1}{R_{33}^2} - \frac{1}{R_{11}^2} \right), & G &= \frac{1}{2} \left(\frac{1}{R_{33}^2} + \frac{1}{R_{11}^2} - \frac{1}{R_{22}^2} \right), \\ H &= \frac{1}{2} \left(\frac{1}{R_{11}^2} + \frac{1}{R_{22}^2} - \frac{1}{R_{33}^2} \right), & L &= \frac{3}{2R_{23}^2}, & M &= \frac{3}{2R_{31}^2}, & N &= \frac{3}{2R_{12}^2} \end{aligned} \tag{16}$$

F, G, H, L, M and N are the Hill’s criterion coefficients. These coefficients are used in FE code as 6 yield stress parameters, R_{11} , R_{22} , R_{33} , R_{12} , R_{13} and R_{23} . These parameters can be calculated by using anisotropic parameters of r_0 , r_{45} and r_{90} from properties of Table 1 as follows

$$\begin{aligned} R_{11} = R_{13} = R_{23} &= 1, & R_{22} &= \sqrt{\frac{r_{90}(r_0 + 1)}{r_0(r_{90} + 1)}}, \\ R_{33} &= \sqrt{\frac{r_{90}(r_0 + 1)}{r_{90} + r_0}}, & R_{12} &= \sqrt{\frac{3r_{90}(r_0 + 1)}{(2r_{45} + 1)(r_{90} + r_0)}} \end{aligned} \tag{17}$$

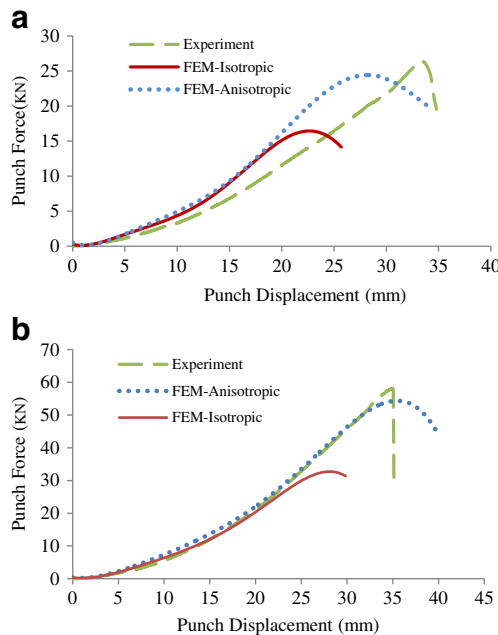


Fig 10 Load- displacement comparison for isotropic and anisotropic sheet with experiment, **a** sheet with 100 mm width, **b** sheet with 150 mm width

Experimental set up for FLD

Weld quality is important for TWB parts, because in the forming process weld should be safe and without any defect. In this work, TWBs were obtained by CO₂ laser welding of IF steel sheets with thickness of 0.77 mm and 1.17 mm. In this welding process no filler material was used. Parameters of CO₂ laser welding were selected such that TWB didn’t fail from weld zone under different forming tests. The weld lines direction in the experimental and FEM samples were perpendicular to the rolling direction of the sheet and also perpendicular to the major strain direction.

Experimental FLD calculation was done by stretch forming tests according to the procedure suggested by Hecker [19] using a hemispherical punch of 101.6 mm diameter on a 200 kN hydraulic press. The schematic arrangement of the tools is

Fig 11 Load–displacement comparison of FEM and experiments for samples with different widths. **a** TWB sample with 25 mm width **b** TWB sample with 75 mm width. **c** TWB sample with 100 mm width **d** TWB sample with 125 mm width. **e** TWB sample with 150 mm width **f** TWB sample with 200 mm width

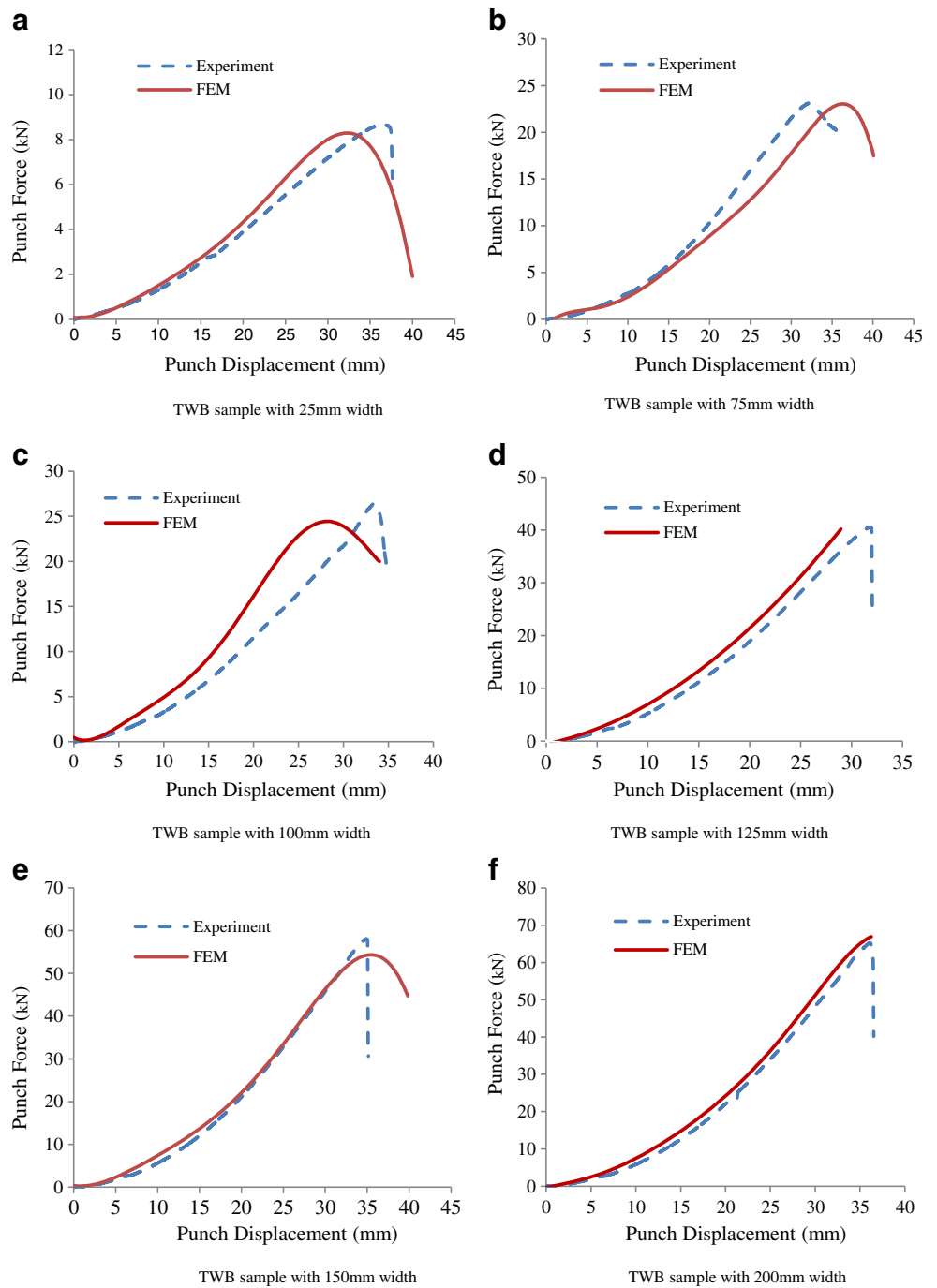


Table 3 LDH (mm) of TWB samples using different criteria

Criterion Sample	FLDcrt	MSFLD	SDT	DFCrt	PMFC	Experiment
25×200	34.81	34.2	33.8	34.6	33.7	36.4
75×200	36.06	35.76	36	35.96	36.1	32
100×200	26.7	26.6	26.3	26.6	27.7	32.5
125×200	26.71	26.81	26.61	26.61	28.65	31.35
150×200	33.19	33.29	33.19	33.09	34.72	34.4
200×200	34.01	34.11	34.01	34.01	35.85	35.65

Table 4 Punch’s maximum force (kN) in the forming of TWB samples using different criteria

Criterion Sample	FLDcrt	MSFLD	SDT	DFCrt	PMFC	Experiment
25×200	7.85	8.73	9.6	8.88	8.52	8.67
75×200	23.9	23.4	23.5	23.1	23.2	22.9
100×200	25.27	24.91	24.05	24.91	25.86	26.02
125×200	35.7	36	35.2	35.3	39.34	40.18
150×200	54.48	54.5	54.48	54.4	55.73	57.38
200×200	63.31	63.67	63.38	63.31	66.7	66.27

Table 5 Criteria which have the best agreement with experimental result for LDH prediction

Sample	25×200	75×200	100×200	125×200	150×200	200×200
Criterion	FLDcrt	MSFLD	PMFC	PMFC	PMFC	PMFC
Deviation (%)	4.4	11.75	14.8	8.6	0.93	0.56

shown in Fig. 7. The experimental setup (punch, die, blank holder and data acquisition system) is shown in Fig. 8.

All tests were conducted in dry condition at a punch speed of 20 mm/min. An optimum blank holding force in the range of 60–100 kN was applied on the upper die. The press was equipped with load and displacement sensors and experiments were stopped when forming load decreased suddenly.

Eight specimens of size 25×200 mm to 200×200 mm were cut from the laser welded specimen such that weld line were perpendicular to the stretching direction (transverse specimens). Specimens were grid marked with circles of 2.5 mm by electrochemical etching method to measure major and minor strains after deformation.

Results and discussion

Load–displacement curves

For mesh sensitivity investigation of modeling in Abaqus, two simulations with different mesh sizes were done for the TWB sample with 125 mm width. The force-displacement curves of the punch are shown in Fig. 9 (Model 1 means mesh size of 1 mm×1 mm and Model 2 means mesh size of 0.5 mm×0.5 mm). Although Model 1 has a rougher mesh when compared to Model 2, its prediction is in good agreement with Model 2 (with finer mesh).

Effect of mesh size was also investigated on the necking time and limit strains for these two models. Data of Table 2 shows that necking time and limit strains prediction of these models are near to each other. Based on these results, for decreasing time computation, model with mesh size of 1 mm×1 mm is used for simulation of all samples.

The load–displacement curves of the TWBs were obtained from data acquisition system during stretch forming in experimental tests. For investigation of the effect of sheet anisotropy on the forming behavior, two samples with 100 mm and 150 mm width were simulated with isotropic behavior for sheet material and they were compared with anisotropic models. Load–displacement comparison of these samples with experimental results is shown in Fig. 10.

Table 6 Criteria which have minimum difference with experimental result for prediction of maximum force

Sample	25×200	75×200	100×200	125×200	150×200	200×200
Criterion	MSFLD	DFCrt	PMFC	PMFC	PMFC	PMFC
Deviation (%)	0.69	0.87	0.61	2.1	2.9	0.65

This figure shows that maximum load as well as maximum punch displacement of isotropic models has lower values than experimental results. This trend was the same for samples with different widths of 100 mm and 150 mm. These results show that sheet's anisotropy has an important influence on the forming behavior of TWB. Material anisotropic modeling shows good correlation with experiments as presented in Fig. 10.

The simulated punch load profiles were compared with experiments being shown in Fig. 11 for different samples widths. Results show that experimental and numerical load–displacement curves are monotonically increasing, reaching a maximum value when fracture occurs, followed by a sudden decrease on drawing force. However, the intensity of force reduction in the experimental curve is more evident than the numerical ones. Figure 11 also indicates that there is a good agreement between numerical investigations and experimental tests, but samples larger than 100 mm have a better parallel with experiment. Punch's maximum force can be a good criterion of prediction of FLD, because numerical load–displacement curves for all samples look closer to experimental results. Therefore, Punch's Maximum Force Criterion (PMFC) is another possible criterion for FLD prediction, which will be also used for comparison. Based on this criterion, when numerical forming force is maximum, then major and minor strains of necking element are used to define a point in forming limit diagram. Necking element for this criterion is the element which has the minimum thickness.

Comparison of limit dome heights (LDH) values for all TWB samples using different forming limit criteria are summarized in Table 3. Predictions of numerical criteria for LDH were a little higher than experimental results for samples with 25 mm and 75 mm width, but for other sample these predictions are close to experiments.

To select a forming machine with suitable capacity, it is essential to evaluate the maximum forming load as accurate as possible. The maximum forming forces obtained from different approaches are given in Table 4.

Table 5 shows the criteria which have the best agreement with experimental results for LDH prediction. Deviation values of this table show that PMFC, MSFLD and FLDcrt

are the criteria that have better agreement with experiment for LDH prediction. Among these three criteria, PMFC has better results for higher number of samples.

Table 6 shows criteria which have the minimum deviation to predict punch’s load for samples with different width. Deviation values of this table show that PMFC, MSFLD and DFCrt are the numerical criteria which have better accuracy for punch load prediction. Comparing deviation values of

Table 7 Comparison of experimental and FEM results for distinct distances between the weld line and failure position

Strain path	Exp. Distance (mm)	FEM Distance (mm)	Error (%)
25 mm×200 mm	15.5	16.2	0.05
125 mm×200 mm	4.4	4.32	0.02
200 mm×200 mm	4	3.74	0.07

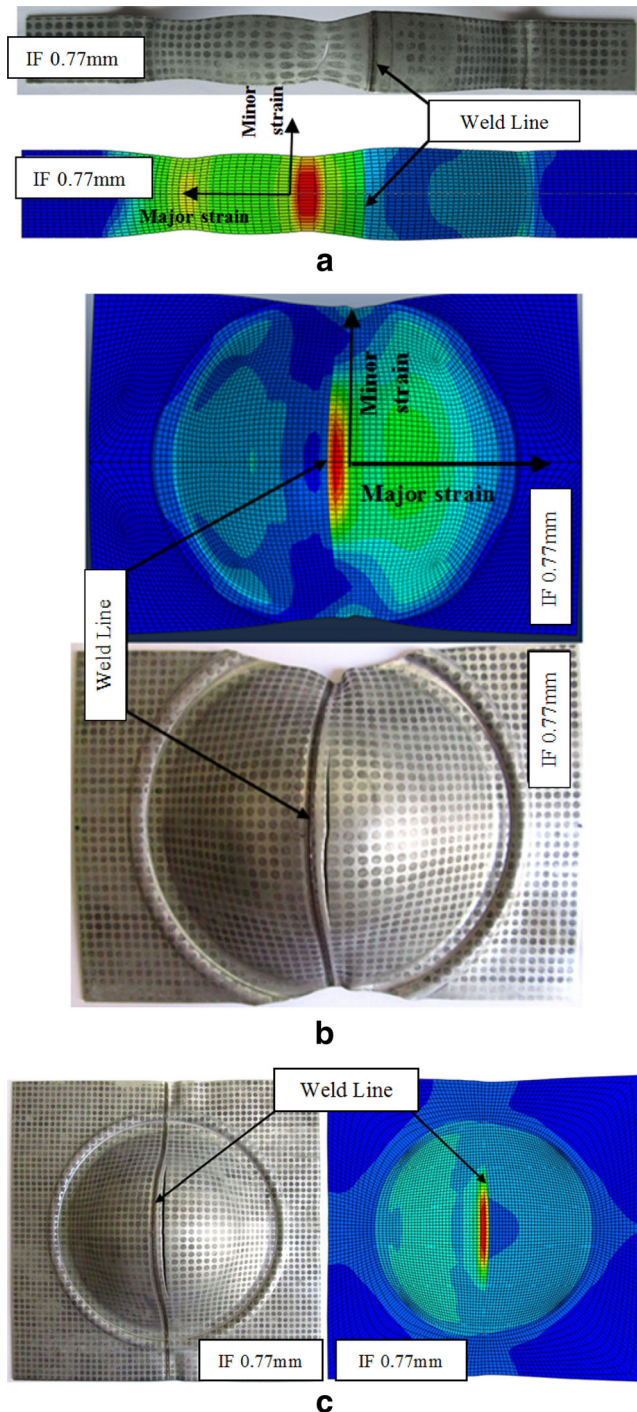


Fig 12 Comparison of necking position for numerical and experimental samples with width of (a) 25 mm, (b) 125 mm, and (c) 200 mm

Table 5 for LDH and deviation values of Table 6 for punch load, it is evident that these numerical criteria show better accuracy for punch load prediction than LDH.

FLD prediction

Prediction of necking location based on presented numerical criteria was the same, since major and minor strains were obtained for the same element of TWB, the only difference among them being on different predictions for forming heights.

Figure 12 shows a comparison between predictions of necking location by different numerical approaches and experiments. Such results are very consistent and necking is always located in the thinner part of TWB, being parallel to the weld line. Distance between the weld line and failure position in the different samples presented in Fig. 12 is compared in Table 7 for FEM and experimental results. Error values of this table show that there is a good agreement between the FEM and experimental results.

Strain values of experimental samples and numerical models near the failure position were compared for two strain paths of 25 mm×200 mm and 125 mm×200 mm. The results presented in Table 8 show that the numerical results have a good agreement with the experimental results for strain prediction.

Figure 13 shows major and minor strains for two samples of 25 mm×200 mm and 125 mm×200 mm. These strains were measured from an element at the pole of the samples and near the fracture zone. Figure 13 shows the distance between the weld line and the element that strains were measured.

Comparison of different numerical criteria for FLD prediction is shown in Fig. 14. Numerical criteria of SDT, MSFLD, FLDcrt and DFCrt can predict only the left side of FLD and are clustered within small strain values in plane strain condition. These numerical criteria are not successful for right side

Table 8 Comparison of experimental and FEM strain values near the failure position

Strain path	Major strain		Minor strain	
	Experimental	FEM	Experimental	FEM
25 mm×200 mm	0.642	0.673	-0.223	-0.254
125 mm×200 mm	0.223	0.245	0.044	0.038

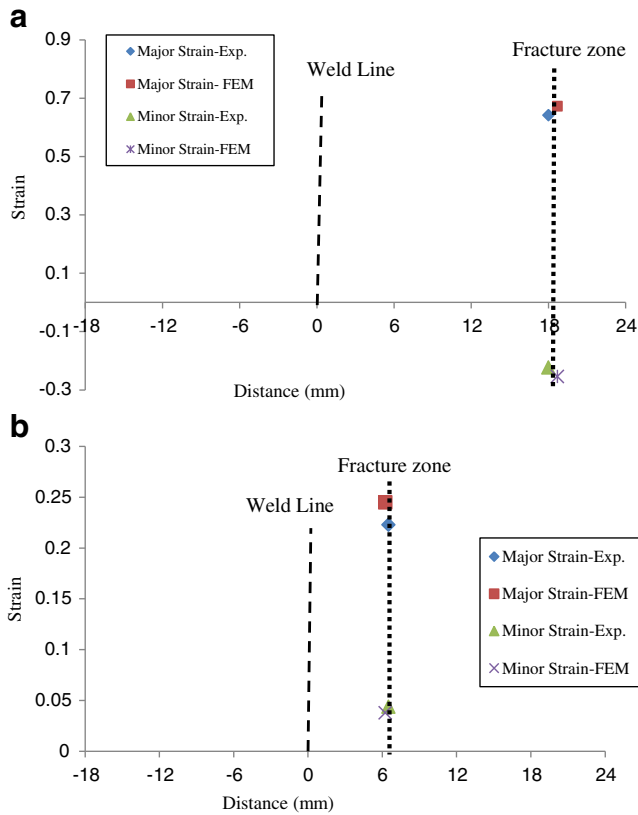
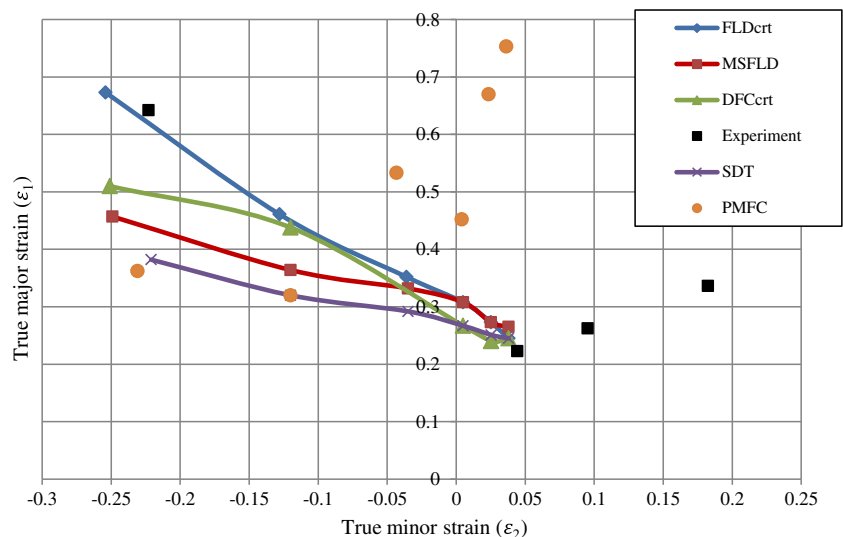


Fig 13 Comparison of experimental and FEM necking strains for two samples of (a) 25 mm×200 mm, (b) 125 mm×200 mm

of FLD and this is the main drawback of presented numerical criteria. This result was mentioned in the Ozturk and Lee [5] studies. Forming limit diagram predicted by FLDert has the best agreement with experimental FLD for $\epsilon_2 < 0$, but for plane strain condition of FLD is over predicted.

Prediction of DFCert is somewhat below experimental FLD, but its prediction in all regions of forming limit diagram is in the safe region. It was expected that DFCert should predict fracture

Fig 14 FLD comparison of IF steel TWB using different numerical criteria



criterion (FLCF, see Fig. 1), but results of this research show that this criterion is able to predict necking limit of forming. Prediction of MSFLD for $\epsilon_2 < 0$ is lower than experiment, but in plane strain condition of FLD is above the experiment. Forming limit of SDT is lower than experiment for $\epsilon_2 < 0$, but in plane strain region its prediction is close to experiment. Although the LDH and punch’s maximum force based on PMFC were close to experiments, its prediction for FLD especially in plane strain region was not completely good.

Conclusions

This paper presents a study on FLD prediction of TWB using different numerical approaches and corresponding validation with experimental results.

Punch load vs. displacement of models simulated with isotropic behavior have lower values than anisotropic models and experimental results, which shows that anisotropy has an important effect on the forming behavior of TWB.

In this study different numerical methods were used to predict the FLD of IF steel TWB. These methods included: Müschenborn and Sonne Forming Limit Diagram (MSFLD), Forming Limit Diagram criterion (FLDert), Second derivative of thinning (SDT) and Ductile Fracture Criteria (DFCert).

Results show that numerical models have good accuracy for punch’s load and LDH. Among these numerical approaches, PMFC has the best accuracy for punch’s load and LDH for most samples with different widths, but its prediction for FLD lacks some accuracy. Forming limit diagram predicted by FLDert criterion has the best agreement with experimental FLD for $\epsilon_2 < 0$, but for plane strain condition has over prediction. DFCert predicts lower results than experimental FLD, locating the prediction of all regions in forming limit diagram in the safe region.

The main drawback of the presented numerical approaches for FLD prediction is the fact of these criteria not succeeding to predict accurately the right side of FLD for TWB and showing the need for further improvements in this topic, namely an improved interface modeling for the boundary between the two different materials.

References

- Han HN, Kim K-H (2003) A ductile fracture criterion in sheet metal forming process. *J Mater Process Technol* 142(1):231–238
- Keeler SP, Backofen WA (1963) Plastic instability and fracture in sheets stretched over rigid punches. *Trans ASM* 56:25–98
- Goodwin GM (1968) Application of strain analysis to sheet metal forming problems in the press shop. SAE Technical Paper: Paper No. 680093
- Jain M, Allin J, Lloyd DJ (1999) Fracture limit prediction using ductile fracture criteria for forming of an automotive aluminum sheet. *Int J Mech Sci* 41(10):1273–1288. doi:10.1016/S0020-7403(98)00070-8
- Ozturk F, Lee D (2004) Analysis of forming limits using ductile fracture criteria. *J Mater Process Technol* 147(3):397–404. doi:10.1016/j.jmatprotec.2004.01.014
- Sheng ZQ (2008) Formability of tailor-welded strips and progressive forming test. *J Mater Process Technol* 205(1–3):81–88. doi:10.1016/j.jmatprotec.2007.11.108
- Shi MF, Pickett KM, Bhatt KK (1993) Formability issues in the application of tailor welded blank sheets. SAE, New York
- Chien WY, Pan J, Tang SC (2004) A combined necking and shear localization analysis for aluminum sheets under biaxial stretching conditions. *Int J Plast* 20(11):1953–1981. doi:10.1016/j.ijplas.2003.08.006
- Chan LC, Chan SM, Cheng CH, Lee TC (2005) Formability and weld zone analysis of tailor-welded blanks for various thickness ratios. *J Eng Mater Technol* 127(2):179–185. doi:10.1115/1.1857936
- Safdarian Korouyeh R, Moslemi Naeini H, Liaghat G (2012) Forming limit diagram prediction of tailor-welded blank using experimental and numerical methods. *J Mater Eng Perform* 21(10):2053–2061. doi:10.1007/s11665-012-0156-9
- Safdarian Korouyeh R, Moslemi Naeini H, Torkamany MJ, Liaghat G (2013) Experimental and theoretical investigation of thickness ratio effect on the formability of tailor welded blank. *Optics Laser Technol* 51(0):24–31. doi:10.1016/j.optlastec.2013.02.016
- Müschelborn W, Sonne H (1975) Influence of the strain path on the forming limits of sheet metal. *Arch für das Eisenhüttenwesen* 46(2):597–602
- (ASTM) ASfTaM (1999) Metals Test Methods and Analytical Procedures
- Brun R, Chambard A, Lai M, De Luca P (1999) Actual and virtual testing techniques for a numerical definition of materials. In: Numisheet International Conference. BURS, pp 393–400
- Panda SK, Kumar DR, Kumar H, Nath AK (2007) Characterization of tensile properties of tailor welded IF steel sheets and their formability in stretch forming. *J Mater Process Technol* 183(2–3):321–332. doi:10.1016/j.jmatprotec.2006.10.035
- He S, Wu X, Hu SJ (2003) Formability enhancement for tailor-welded blanks using blank holding force control. *J Manuf Sci Eng* 125(3):461–467. doi:10.1115/1.1580853
- Saunders FI, Wagoner RH (1996) Forming of tailor-welded blanks. *Metall Mater Trans A* 27(9):2605–2616. doi:10.1007/bf02652354
- Hill R (1948) A theory of the yielding and plastic flow of anisotropic metals. *Proc Royal Soc Lond Ser A Math Phys Sci* 193(1033):281–297. doi:10.1098/rspa.1948.0045
- Hecker SS (1974) A cup test for assessing stretchability. *Met Eng* 14:30–36